$\sim 10^3$ it seems likely that a cluster will absorb more than one photon. If this is so, one may then understand why we did not observe any "positive" signal associated with large clusters having a rate of photoevaporation low enough to survive passage from the excitation region to the bolometer.

We ascribe the smooth red shift in absorption maximum shown by spectra 6A–C to a steady increase in the mean size of the clusters. The widths of the spectra are too large to allow resolution of the spectrum of each successive cluster and so a steady shift in the absorption maximum is observed.

Spectra 6D–F are characteristic of the growth of one class of species at the expense of another. They signify a discontinuity in the clustering process which we tentively assign as a structural rearrangement occurring once the clusters reach a critical size. Such a rearrangement occurs because the most stable arrangement of a limited number of molecules is, in general, not the same as the molecular disposition within the unit cell which is the repeating unit of an extended solid. Several studies of metal clusters, using electron diffraction molecular beam techniques,[26] have revealed evidence which supports the idea of a critical cluster size.

The interpretation of spectra 6D–F contains a serious weakness; the second peak at 3709.3 $cm^{-1}$ is shifted beyond the position of the $\nu_1 + \nu_3$ of solid carbon dioxide. In fact, the valley between the two peaks coincides, to the accuracy of our measurements, with the absorption of the solid. A similar coincidence for nitrous oxide may be found upon inspection of Figure 2 of ref 8.

Although considerable theoretical work[27] has been carried out to establish the growh sequence of rare gas clusters, such as argon, no detailed calculations exist for the case of clusters formed from molecules. Adding to the complexity of the problem is the fact that infrared spectrum depends not only on the ground state properties but also those in the excited vibrational state. A considerable amount of theoretical work will therefore be required before these spectra can be fully interpreted. However, these results do show that much more information is available than simply the gas- and solid-state spectra. Indeed, the investigation of these "intermediate phases" should, in the future, be extremely useful in the study of many-body forces as well as the details of condensation phenomena.

(26) A. Yokozeki and G. D. Stein, *J. Appl. Phys.*, **49**, 2224 (1978); J. C. Allpress and J. V. Sandors, *Surf. Sci.*, **7**, 1 (1967).

(27) C. L. Briant and J. J. Burton, *J. Chem. Phys.*, **63**, 2045 (1975); M. R. Hoare and P. Pal, *J. Cryst. Growth*, **16**, 77 (1972).

# A Reaction Path for Halogen Elimination from $CX_2Y_2$, and Its Dynamical Implications

**Stephen R. Cain, Roald Hoffmann,* and Edward R. Grant***

*Department of Chemistry, Cornell University, Ithaca, New York 14853* *(Received: July 7, 1981; In Final Form: September 9, 1981)*

A qualitative molecular orbital exploration of the reaction path for $CX_2Y_2 \rightarrow CY_2 + X_2$ is presented. The least-motion departure is symmetry forbidden and a less symmetrical path is implicated, one likely to result in substantial rotational excitation of the products. The smaller the HOMO–LUMO gap in the expelled dihalogen $X_2$, the smaller should be the reaction barrier and the degree of rotational excitation of the products.

The elimination of a diatomic molecule upon thermal or photochemical excitation of a substituted methane, **1**,

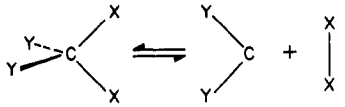

**1**

is of course the reverse of the addition of a carbene to a single bond. That reverse reaction, carbene insertion, has a long experimental and theoretical history.[1-4] Surfaces for carbene insertion into hydrogen,[2] C–H bonds,[3,4c,h] and carbon–carbon double bonds[4] have been studied in detail. The forward reaction, specifically for the case of halogen substituents, is of current experimental interest.[5] For this reason we have undertaken a qualitative theoretical exploration of the reaction for X = Y = halogen.

## The Least-Motion Path

There is much understanding to be gained from a qualitative orbital-symmetry based analysis of this reac-

(1) See, for example, (a) "Carbenes", M. Jones and R. A. Moss, Ed., Vol. I, Wiley, New York, 1973; (b) "Carbenes", M. Jones and R. A. Moss, Ed., Vol. II, Wiley, New York, 1975; (c) "Carbene Chemistry", W. Kirmse, Ed., Vol. I, 2nd ed, Academic Press, New York, 1971.

(2) (a) H. Kollmar, *Tetrahedron*, **28**, 5893 (1972); (b) J. N. Murrell, J. B. Pedley, and S. Durmaz, *J. Chem. Soc., Faraday Trans. 2*, **69**, 1370 (1973); (c) P. Cremaschi and M. Simonetta, *ibid.*, **70**, 1801 (1974); (d) C. W. Bauschlicher, Jr., H. F. Schaefer, III, and C. F. Bender, *J. Am. Chem. Soc.*, **98**, 1653 (1976); (e) C. W. Bauschlicher, Jr., K. Haber, H. F. Schaefer, III, and C. F. Bender, *ibid.*, **99**, 3610 (1977); (f) M. S. Gordon, *Chem. Phys. Lett.*, **52**, 161 (1977); (g) H. Kollmar, *J. Am. Chem. Soc.*, **100**, 2660 (1978); (h) D. Jeziorek and B. Zurawski, *Int. J. Quant. Chem.*, **16**, 277 (1979); (i) H. Kollmar and V. Staemmler, *Theor. Chim. Acta*, **51**, 207 (1979); (j) M. S. Gordon and J. W. Caldwell, *J. Chem. Phys.*, **70**, 5503 (1979); (k) H. U. Lee and R. Janoschek, *Chem. Phys.*, **39**, 271 (1979).

(3) R. C. Dobson, D. M. Hayes, and R. Hoffmann, *J. Am. Chem. Soc.*, **93**, 6188 (1971).

(4) (a) A. G. Anastassiou, *Chem. Commun.*, 991 (1968); (b) R. Hoffmann, *J. Am. Chem. Soc.*, **90**, 1475 (1968); (c) N. Bodor, M. J. S. Dewar, and J. Wasson, *ibid.*, **94**, 9095 (1972); (d) T. Fueno, S. Nagase, K. Tatsumi, and K. Yamaguchi, *Theor. Chim. Acta*, **26**, 43 (1972); (e) H. Fujimoto, S. Yamabe, and K. Fukui, *Bull. Chem. Soc. Jpn.*, **45**, 2424 (1972); (f) R. Hoffmann, D. M. Hayes, and P. S. Skell, *J. Phys. Chem.*, **76**, 664 (1972); (g) H. Fujimoto and R. Hoffmann, *ibid.*, **78**, 1167 (1974); (h) S. Nagase and T. Fueno, *Theor. Chim. Acta*, **41**, 59 (1976); (i) W. W. Schoeller and E. Yurtsever, *J. Am. Chem. Soc.*, **100**, 7548 (1978); (j) B. Zurawski and W. Kutzelnigg, *ibid.*, **100**, 2654 (1978); (k) N. G. Rondan, K. N. Houk, and R. A. Moss, *ibid.*, **102**, 1770 (1980); (l) S. Y. Chu, A. K. Q. Siu, and E. F. Hayes, *ibid.*, **94**, 2969 (1972).

(5) See, for example, (a) P. A. Schulz, Aa. S. Sudbø, D. J. Krajnovich, H. S. Kwok, Y. R. Shen, and Y. T. Lee, *Annu. Rev. Phys. Chem.*, **30**, 379 (1979); (b) R. J. S. Morrison and E. R. Grant, *J. Chem. Phys.*, **71**, 3537 (1979); (c) R. J. S. Morrison, R. F. Loring, R. L. Farley, and E. R. Grant, ibid., in press.

0022-3654/81/2085-4046$01.25/0 

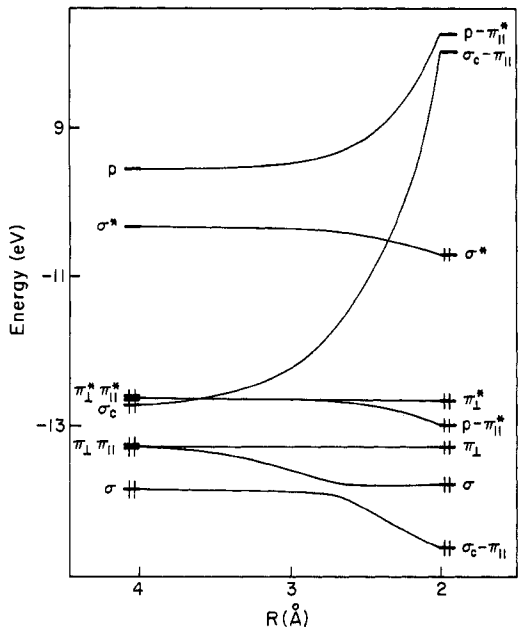


**Figure 1.** Correlation diagram for the "least-motion" attack.

tion. What follows is such a study, based on frontier orbital interactions and correlation diagrams, supported by extended Hückel calculations whose details are given in the Appendix. Because the frontier orbitals of carbenes and $X_2$ are so clearly displayed, it makes sense to structure the flow of the analysis in the reverse of **1**, from carbene and halogen diatomic to substituted methane. This we will do, reversing the reaction at the very end to reach some experimentally testable conclusions.

Let us first examine the most obvious path for carbene insertion, the least-motion $C_{2v}$ approach **2** of $CF_2$ to $Cl_2$. This will turn out to be a high energy route. But a detailed examination of the orbitals at fault in **2** will allow us to

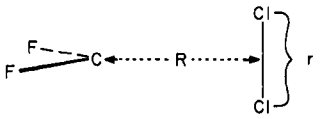


**2**

design a strategy for stabilizing the transition state of the reaction. And the least-motion path will also be "remembered" in the evolution of the orbitals along the energetically less-costly routes.

For a frozen carbene geometry, justified by the similarity of the $CF_2$ fragment geometries in reactant and product, two distances, $r$ and $R$ in **2**, describe the approach. A correlation diagram for $r$ fixed at the equilibrium Cl–Cl separation is shown in Figure 1.

The carbene and halogen frontier orbitals which appear in the correlation diagram are well-known. Since they figure repeatedly in the analysis it is perhaps worthwhile to draw them out schematically here. The carbene carries an in-plane hybrid, called $\sigma_c$, and a p orbital, mainly on the carbene carbon, but slightly destabilized by interaction with fluorine lone pairs, **3**. The important chlorine orbitals, given in **4**, are the familiar $\sigma(\sigma_g)$ and $\sigma^*(\sigma_u)$ and the $\pi(\pi_u)$ and $\pi^*(\pi_g)$ of any diatomic. We distinguish the components of $\pi$ and $\pi^*$ as $\pi_\parallel$ and $\pi_\perp$, where the parallel and perpendicular labels refer to the plane containing the carbon and the two chlorines.

There is a level crossing along this reaction path, i.e., this is a forbidden reaction. Hardly a surprising result, given simple orbital symmetry ideas.[7] But let us examine

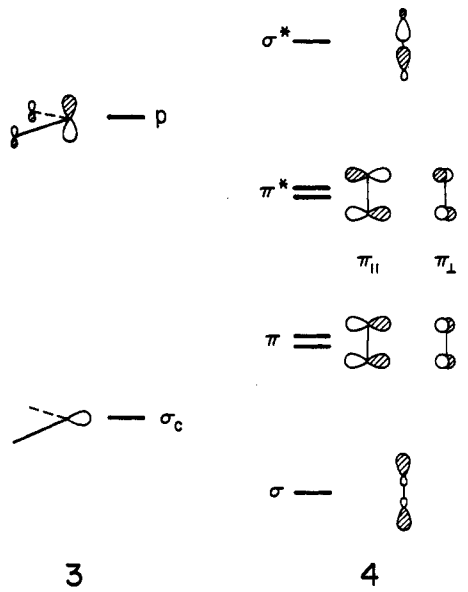


**3** **4**

the correlation diagram in some more detail to evolve a strategy for ameliorating the forbiddenness.

$\sigma^*$, $\sigma$, $\pi_\perp^*$, and $\pi_\perp$ correlate to chlorine lone-pair-like orbitals, while the carbene $\sigma_c$ and p orbitals and $\pi_\parallel$ and $\pi_\parallel^*$ correlate to carbon–chlorine bonding and antibonding orbitals. This remains true even with the more asymmetric paths to be discussed. The primary actors in the level crossing are thus carbene $\sigma_c$ and p and chlorine $\pi_\parallel$, $\pi_\parallel^*$, and $\sigma^*$. The high symmetry of the situation restricts interaction among these to $\sigma_c-\pi_\parallel$ and $p-\pi_\parallel^*,\sigma^*$, drawn in **5**.

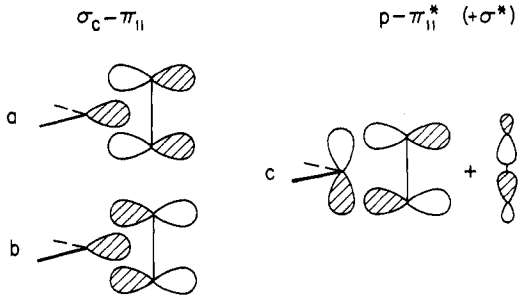


**5**

The $p-\pi_\parallel^*$ interaction is a two-electron, attractive one, while both $\sigma_c$ and $\pi_\parallel$ are occupied, leading to a four-electron destabilization. Detailed examination of the fragment overlaps reveals what is already inferred from Figure 1—the repulsive four-electron interaction dominates. The antibonding component **5a** is destabilized, sent up in energy.

The level crossing that occurs is between $\sigma_c-\pi_\parallel$ (**5a**) and a level descended from chlorine $\sigma^*$, with some carbene p admixture. Drastic changes in the electron distribution of course accompany the level crossing, as may be seen in Figure 2. Transfer of two electrons from **5a**, C–Cl antibonding, Cl–Cl bonding to $\sigma^*$ + p, Cl–Cl antibonding, breaks the Cl–Cl bond, and forms the C–Cl bonds. If $r$ were optimized along the reaction path the Cl–Cl bond length would, of course, increase on the large $R$ side of the crossing.[8]

(6) (a) J. F. Harrison in "Carbene Chemistry", W. Kirmse, Ed., Vol. I, 2nd ed, Academic Press, New York, 1971, pp 159–192; (b) P. P. Gaspar and G. S. Hammond in "Carbenes", M. Jones and R. A. Moss, Ed., Vol. II, Wiley, New York, 1975, pp 207–362; (c) R. Hoffmann, G. D. Zeiss, and G. W. Van Dine, *J. Am. Chem. Soc.*, **90**, 1485 (1968).

(7) R. B. Woodward and R. Hoffmann, *Angew. Chem., Int. Ed. Engl.*, 8, 781 (1969).

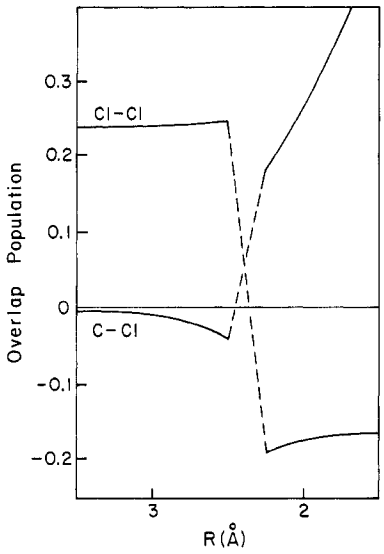


**Figure 2.** Overlap populations indicate formation of C–Cl bonds and scission of the Cl–Cl bond. The initial decrease in C–Cl overlap population points to some initial fragment repulsion.

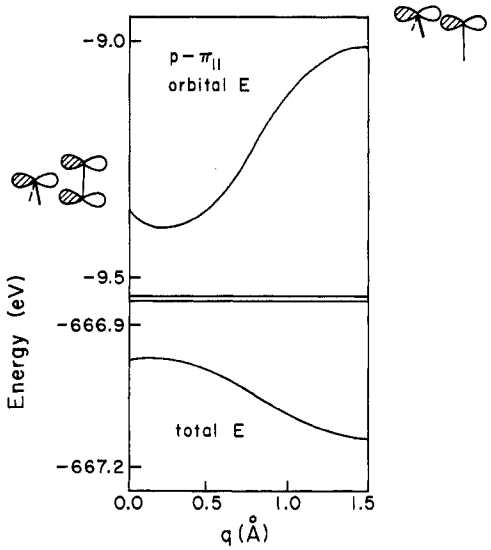


**Figure 3.** Slip off center: system stabilization by the empty p–$\pi_\parallel$ orbital.

A final point is that the height of the least-motion barrier can be related to the HOMO–LUMO gap of the halogen. If the $\pi^*$ orbital is raised, it interacts better with the p orbital. This is a two-center, two-electron attractive interaction. Hence the better this interaction, the lower the barrier. If the $\sigma^*$ orbital is lowered, the crossing takes place sooner, hence the lower the barrier. Putting the two together: the smaller the halogen HOMO–LUMO gap, the smaller the least motion barrier to reaction. We shall see that this "rule" holds even for more asymmetric paths.

Let us now investigate other geometries for the initial attack.

## Approaching the Reaction Pathway

Carbenes are potentially ambiphilic[9]—one can think it is the geometry of attack, **6**, which governs whether the

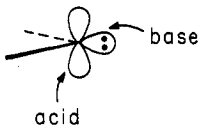


**6**

carbene will act as a base, nucleophile, or an acid, electrophile. Attack at carbon from above or below the plane of the carbene implies that the carbene acts as an acid. Attack from the front of the carbene implies that the carbene acts as a base. Since halogen molecules are electron-rich, we reason that it would be best to utilize the acidic character of the carbene.[10] This can be done by keeping the plane of the carbene parallel to the Cl–Cl bond. In fact, we can define an angle, $\theta$ (see **7**), which

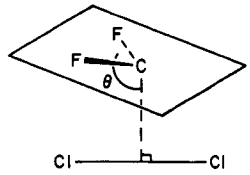


**7**

"parameterizes" the acid–base nature of the carbene in the initial attack. ($\theta = 90° \rightarrow$ acid, $\theta = 180° \rightarrow$ base.) At a distance of $R = 2.5$ (shortly before the HOMO–LUMO crossing) we find that $\theta$ prefers to be 90°. The energy of the HOMO decreases steadily from $\theta = 180$ to 90°, and so does the total energy of the system. All orbitals but the HOMO remain essentially constant in energy. The decrease in energy is due primarily to the decrease in overlap between the $\sigma_c$ orbital and the chlorine $\pi_\parallel$ orbital. In addition to this, we see an increase in the occupation of the p orbital. This indicates a better acid–base interaction between the carbene and chlorine. So by decreasing $\theta$ from 180 to 90°, we (1) decrease the repulsive $\sigma_c$–$\pi_\parallel$ interaction, and (2) increase the attractive p–$\pi_\parallel$ interaction. Rotation essentially has interchanged the spatial orientation of the carbene $\sigma$ and p orbitals from the least-motion path.

We have kept the carbene carbon equidistant from the chlorines. Perhaps we can "gain" even more if we allow the carbene to slip off center from the chlorine–chlorine bond. The coordinate $q$ for such a motion is defined in **8**. A complete correlation diagram can be constructed for

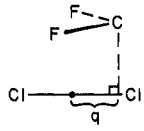


**8**

such a motion, but it is a complicated one. The stabilization of the reaction path is spread out over a number of orbitals; it is mirrored most clearly in the empty p–$\pi_\parallel$ antibonding orbital also shown in Figure 3.

(8) The Cl–Cl distance in $CF_2Cl_2$ is 2.9 Å (L. O. Brockway, *J. Phys. Chem.*, **41**, 747 (1937)), while the Cl–Cl distance in $Cl_2$ is 2.0 Å (L. Pauling and L. O. Brockway, *J. Chem. Phys.*, **2**, 867 (1934)).

(9) See, for example: (a) L. W. Christensen, E. E. Waal, and W. M. Jones, *J. Am. Chem. Soc.*, **94**, 2118 (1972); (b) R. A. Moss, M. Fedorynski, and W. Shieh, *ibid.*, **101**, 4736 (1979).

(10) Carbenes do behave as acids: (a) P. S. Skell and M. S. Cholod, *J. Am. Chem. Soc.*, **91**, 7131 (1969); (b) E. W. Duck, J. M. Locke, and S. R. Wallis, *J. Chem. Soc. C*, 2000 (1970); (c) R. A. Moss, *J. Am. Chem. Soc.*, **94**, 6004 (1972); (d) R. R. Kostikov, A. F. Khlebnikov, and K. A. Ogloblin, *J. Org. Chem. USSR*, **9**, 2369 (1973); (e) R. R. Kostikov, I. A. Vasil'eva, and Ya. M. Slobodin, *ibid.*, **10**, 2339 (1974); (f) E. V. Couch and J. A. Landgrebe, *J. Org. Chem.*, **40**, 1636 (1975); (g) R. A. Moss and C. B. Mallon, *J. Am. Chem. Soc.*, **97**, 344 (1975); (h) R. A. Moss and D. J. Smudin, *J. Org. Chem.*, **41**, 611 (1976); (i) R. A. Moss, C. B. Mallon, and C. Ho, *J. Am. Chem. Soc.*, **99**, 4105 (1977).

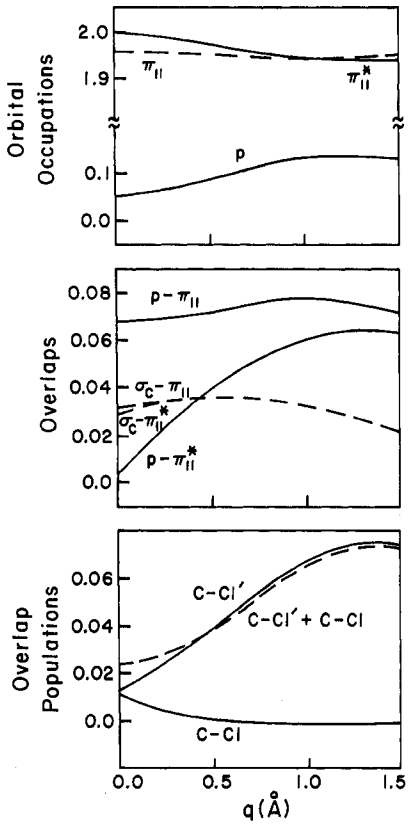


**Figure 4.** Orbital occupations of selected orbitals, some overlaps and resulting overlap populations for the motion of slipping off center.

The increase in this orbital energy is accompanied by a decrease in the total energy. This suggests that this empty orbital pushes down one or more filled orbitals as the carbene carbon slips off the center of the Cl–Cl bond. The polarization of the chlorine $\pi$ contribution to the p–$\pi_{\|}$ orbital suggests the reason for a tendency to slip off center. In order to polarize the $\pi$ bond, we must mix $\pi$ and $\pi^*$ orbitals, as shown for the extreme case of equal mixing in **9**. So we mix more and more $\pi^*$ into this orbital as we

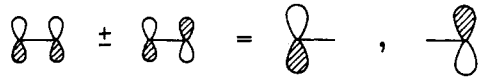

**9**

increase $q$. Since the mixture of $\pi$ and $\pi^*$ gives a more localized orbital, the mixing with p is better, implying in turn more charge transfer to the carbene. This is evident in the fragment orbital occupations shown in Figure 4, top. Note the decrease in the $\pi^*$ occupation and the increase in the p occupation. This is consistent with the notion of an increasing acid–base interaction, where p is the acid and $\pi^*$ is the base. The increasing overlap of p with $\pi^*$ as $q$ increases accounts for this. The middle of Figure 4 shows that this overlap changes more substantially than the other pertinent overlaps. The differential is easily traced to the orbital shapes, **10**. The carbene feels no nodes from the $\pi_{\|}$ orbital. It samples the node of the $\pi^*_{\|}$ orbital when $q$ is zero, but becomes less affected by the node as $q$ increases. That the slip off center aids in net formation of a carbon chlorine bond is shown by the overlap populations at the bottom of Figure 4.

From the above discussion we conclude that the carbene attacks in an acidic fashion at one of the chlorines. This jibes with the less sophisticated "Lewis electron dot" picture of an acid attacking the chlorine "lone pairs", **11**.

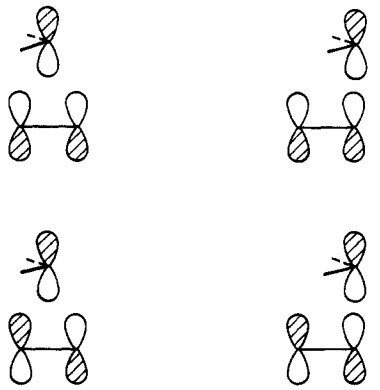

**10**

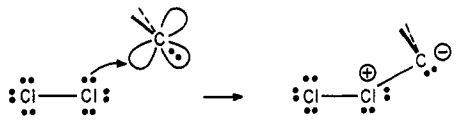

**11**

Since we now have a rough picture of the geometry of the initial attack, we can define suitable coordinates for finding the optimum geometry, **12**.

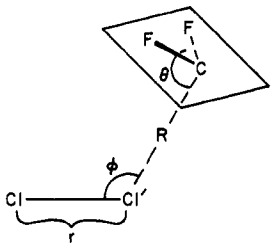


**12**

For $R \geq 2.75$ the optimum approach was located at approximately $\theta = 100°$, $\phi = 145°$, $r = 2.55$ Å, which is approximately the geometry illustrated in **12**. The surface is quite hard with respect to the coordinate $\theta$. This is due to the repulsions of carbene $\sigma$ with the chlorines as $\theta$ increases from 100°, and the repulsion of the carbene fluorines with the chlorines as $\theta$ decreases. This is supported by the increasing negative overlap population between C and Cl′ as $\theta$ increases to 180° and the increasing negative overlap population between F and Cl as $\theta$ decreases. On the other hand, except for the avoidance of the nodal plane of the $\pi^*$ orbital, the surface with respect to $\phi$ is quite soft.

It is informative to follow the population analysis along the initial approach ($\theta = 100°$, $\phi = 145°$, $R$ decreasing from $\infty$). Figure 5 shows the results. There is a charge transfer from the chlorine $\pi$ and $\pi^*$ to the p orbital, resulting in incipient C–Cl′ bond formation. The electrons for this transfer come from Cl′ as a consequence of the previously discussed $\pi$-bond polarization. Finally, since electrons are transferred from $\pi$ and $\pi^*$ about equally, there is no substantial change in the Cl–Cl bond order, accounting for the constancy of the Cl–Cl′ distance. The simple Lewis-dot picture **11** accounts for these results.

A consequence of the acceptor–donor picture of the early stages of the reaction is that one would predict a low barrier for torsion around the Cl′–C axis in **12**. This is indeed so even when the two reactants are fairly close ($R \geq 2.5$ Å).

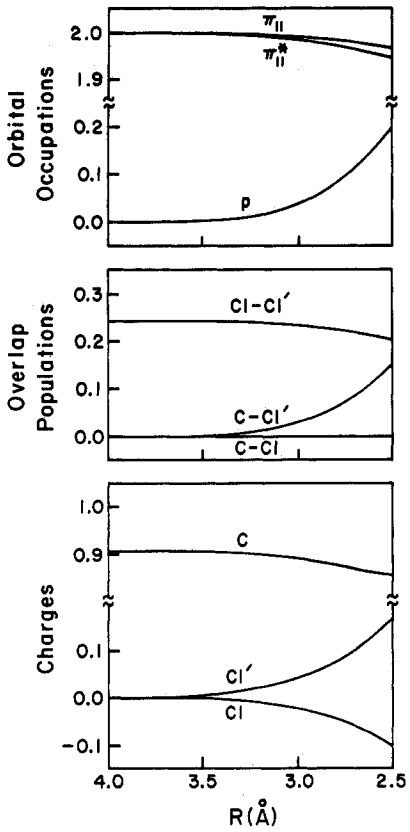


**Figure 5.** Asymmetric attack: charges and populations indicate strong acid–base interaction between the fragments.

## The Completed Reaction Path and Experimental Conclusions

Now we must complete the reaction. A linear transit from a geometry on the $\pi$ approach to the product was taken, i.e., C–Cl, C–Cl′, Cl–Cl′, and Cl–F bond distances were varied synchronously in linear increments. The assumed transit is illustrated in a series of superimposed snapshots in **13**.

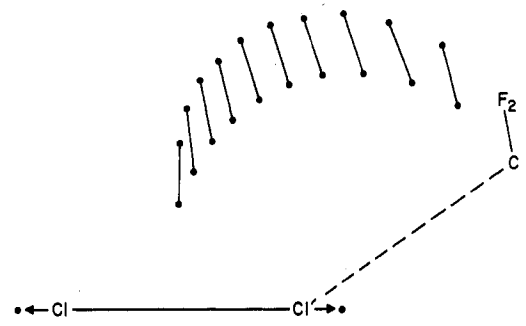


**13**

A correlation diagram showing the evolution of the orbitals may be found in Figure 6. Once again the $\sigma^*$-, $\sigma$-, $\pi_\perp{}^*$-, and $\pi_\perp$-like orbitals correlate to chlorine lone pairs, and $\sigma_c$-, p-, $\pi_\parallel$-, and $\pi_\parallel{}^*$-like orbitals to C–Cl bonds and antibonds. So this is the same picture as for the least-motion path, perturbed only by some avoided crossing. That is, the system "remembers" the features of the least-motion path, even for very asymmetric reaction paths.

We now focus on the HOMO–LUMO interaction, since it is principally responsible for holding down the barrier of rearrangement to the final product. The motion toward

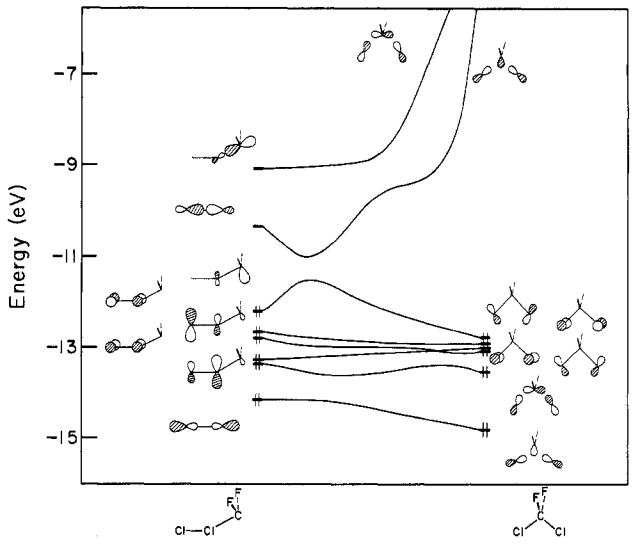


**Figure 6.** Correlation diagram for the completion of the reaction.

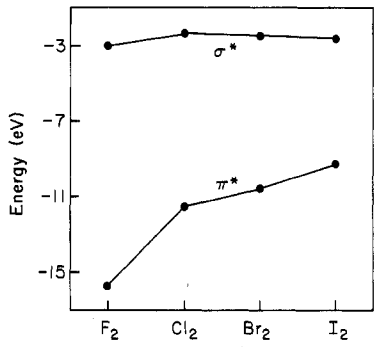


**Figure 7.** Halogen orbital energies from ionization potential and electron affinity data.

the final product involves two unfavorable movements: (1) rotation of the carbene lone pair into the electron density of the Cl–Cl bond, and (2) stretching of the Cl–Cl bond. These two motions, however, aid each other. As the lone pair rotates into the Cl–Cl bond, it begins to interact with the $\sigma^*$ orbital. This is suggested by the decrease in overlap population of the Cl–Cl bond, even for a path in which the Cl–Cl distance was fixed at 2.55 Å throughout the course of the motion. Hence, it becomes easier to stretch the Cl–Cl bond. But stretching the Cl–Cl bond lowers the $Cl_2$ $\sigma^*$ orbital so it can interact better with the carbene $\sigma$ keeping the HOMO low in energy. Now, the better $\sigma^*$ carbene $\sigma$ mixing causes the $\sigma^*$ orbital to be occupied more, so it is even easier to stretch the Cl–Cl bond. And so on. Hence we conclude that, though the system "remembers" the forbiddenness of the least-motion path, it effectively "sidesteps" the least-motion barrier by attacking in an asymmetrical fashion. The least-motion barrier was found to be about three times the barrier for an asymmetrical initial attack.

The barrier can be lowered further by decreasing the HOMO–LUMO gap. Since we wish to confine ourselves to a specific carbene ($CF_2$) we can only change the diatomic halogen fragment. The smaller the *halogen* HOMO–LUMO gap, the smaller the *system* HOMO–LUMO gap, hence the smaller the barrier to the reaction. Note that this is the same rule as for the least-motion barrier, even though the reasoning is a bit different.

We are at the point where we can make some predictions based on these results and some experimental parameters. As mentioned above, the barrier to the reaction correlates with the size of the halogen HOMO–LUMO gap. Figure

TABLE I: Extended Hückel Coulomb Integrals ($H_{ii}$) and Slater Exponents

| | $H_{ii}$, eV | exponent |
|---|---|---|
| C 2s | −21.4 | 1.625 |
| C 2p | −11.4 | 1.625 |
| Cl 3s | −30.0 | 2.0 |
| Cl 3p | −13.0 | 2.0 |
| F 2s | −40.0 | 2.425 |
| F 2p | −18.0 | 2.425 |

7 shows the ionization potentials and electron affinities of the halogens.[11] Assuming Koopmans theorem this places the $\pi^*$ and $\sigma^*$ orbitals. Since the HOMO–LUMO gap decreases as we go from $Cl_2$ to $I_2$, we conclude that the barrier to insertion should decrease as we go from $Cl_2$ to $I_2$. This is in accord with the results of multiphoton dissociation experiments for $CF_2Cl_2$[5b] and $CF_2Br_2$.[5c] Work is currently under way for the $CF_2I_2$ system.[12]

Information about reaction dynamics can be inferred from the potential energy surface. Since a low-energy path involves an asymmetrical intermediate, we can imagine that a significant fraction of any energy released as the fragments separate will appear as internal excitation of the products. A crude estimate of the extent of this expected excitation can be derived from the properties of the potential energy surface.

Taking our transition state as the initial geometry in **13**, and recalling the previous arguments about the geometry of the initial attack, we see that the gradient of the potential (toward the lower energy of separated fragments) will be steepest for a displacement along the C–X coordinate. The asymmetry of this force with respect to the centers of mass of the incipient fragments will result in the deposition of much of the energy associated with this coordinate into $X_2$ and $CF_2$ rotation. For an insertion barrier of a few kcal/mol, we can thus expect fragment rotational distributions rather hotter than room temperature.

The final vibrational energy of $X_2$ product will depend on coupling of exit channel relaxation with the X–X relative motion. Since formation of the X–X bond occurs fairly early in the dissociation (scission is late in the insertion), the $X_2$ coordinate will be substantially relaxed in the critical configuration and we expect vibrational excitation to be less than rotational excitation.

From the above, we predict that the higher the barrier to insertion, the higher the rotational excitation of dissociated products relative to vibrational and translational excitation. Hence we expect the ratio of rotational excitation to vibrational and translation excitation to decrease as X changes from Cl to Br to I.

These predictions are testable by molecular beam experiments. Such experiments are now under development. For a thorough comparison of experimental and theoretically predicted dynamics, the qualitative features of the surface discussed in this paper provide the basis for a more complete surface on which trajectory calculations can be conducted. Such calculations are currently under way.

*Acknowledgment.* We are grateful to the National Science Foundation for its support of this work through Research Grant CHE 7828048.

## Appendix

In the extended Hückel calculations[13] we used the parameters given in Table I.

(11) Electron affinities: W. A. Chupka, J. Berkowitz, and D. Gutman, *J. Chem. Phys.*, **55**, 2725 (1971). Ionization potentials: (a) R. P. Iczkowski and J. L. Margrave, *J. Chem. Phys.*, **30**, 403 (1959); (b) K. Watanabe, T. Nakayama, and J. Mottl, *J. Quantum Spectrosc. Radiat. Transfer*, **2**, 369 (1962); (c) I. P. Fisher, J. B. Homer, and F. P. Lossing, *J. Am. Chem. Soc.*, **87**, 957 (1965).

(12) S. Cain, R. J. S. Morrison, and E. R. Grant, to be published.

(13) R. Hoffmann and W. N. Lipscomb, *J. Chem. Phys.*, **36**, 2179 (1962).

# Studies in the Vibrational Spectroscopy of Sodium Trioxodinitrate[1]

**Francis T. Bonner,* Mohammad Javaid Akhtar, Tseng-Ven King, Li-Heng Chen, and Takanobu Ishida***

*Department of Chemistry, State University of New York at Stony Brook, Stony Brook, New York 11794* *(Received: July 14, 1981; In Final Form: September 11, 1981)*

Infrared and Raman spectra are reported for sodium trioxodinitrate, $Na_2N_2O_3$, including nitrogen isotope shifts for the isotopic forms $Na_2O^{15}NNO_2$, $Na_2ON^{15}NO_2$ and $Na_2O^{15}N^{15}NO_2$, and solution Raman spectra exhibiting the effects of monoprotonation on the $N_2O_3^{2-}$ anion. A normal coordinate analysis has been carried out by the Wilson **GF**-matrix method, and the complex motions corresponding to the nine fundamentals are characterized in detail. A hitherto unreported out-of-plane fundamental at 210 $cm^{-1}$ was predicted in the course of the calculation and subsequently observed.

Sodium trioxodinitrate ("Angeli's salt"[2]), $Na_2N_2O_3$, has been the subject of a number of structural studies, among them a brief account of its infrared and Raman spectra by Feltham.[3] The crystallographic study of Hope and Sequeira[4] provided detailed information concerning symmetry, bond angles, and distances, and showed unambiguously that the predominant structural form of the dianion $N_2O_3^{2-}$ is

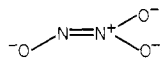

The dianion is stable in aqueous solution, but in the pH range in which the species $HN_2O_3^-$ predominates ($pK_1$ =

(1) Research supported by the National Science Foundation, Grant No. 78-24176, and Division of Basic Energy Sciences, U.S. Department of Energy, Contract No. DEAC02-80ER10612.

(2) Angeli, A. *Gazz. Chim. Ital.* **1896**, *26*, 7.

(3) Feltham, R. D. *Inorg. Chem.* **1964**, *3*, 900.

(4) Hope, H.; Sequeira, M. R. *Inorg. Chem.* **1973**, *12*, 286.

0022-3654/81/2085-4051$01.25/0 